Figures and figure supplements

Sperm chemotaxis is driven by the slope of the chemoattractant concentration field

Héctor Vicente Ramírez-Gómez *et al*

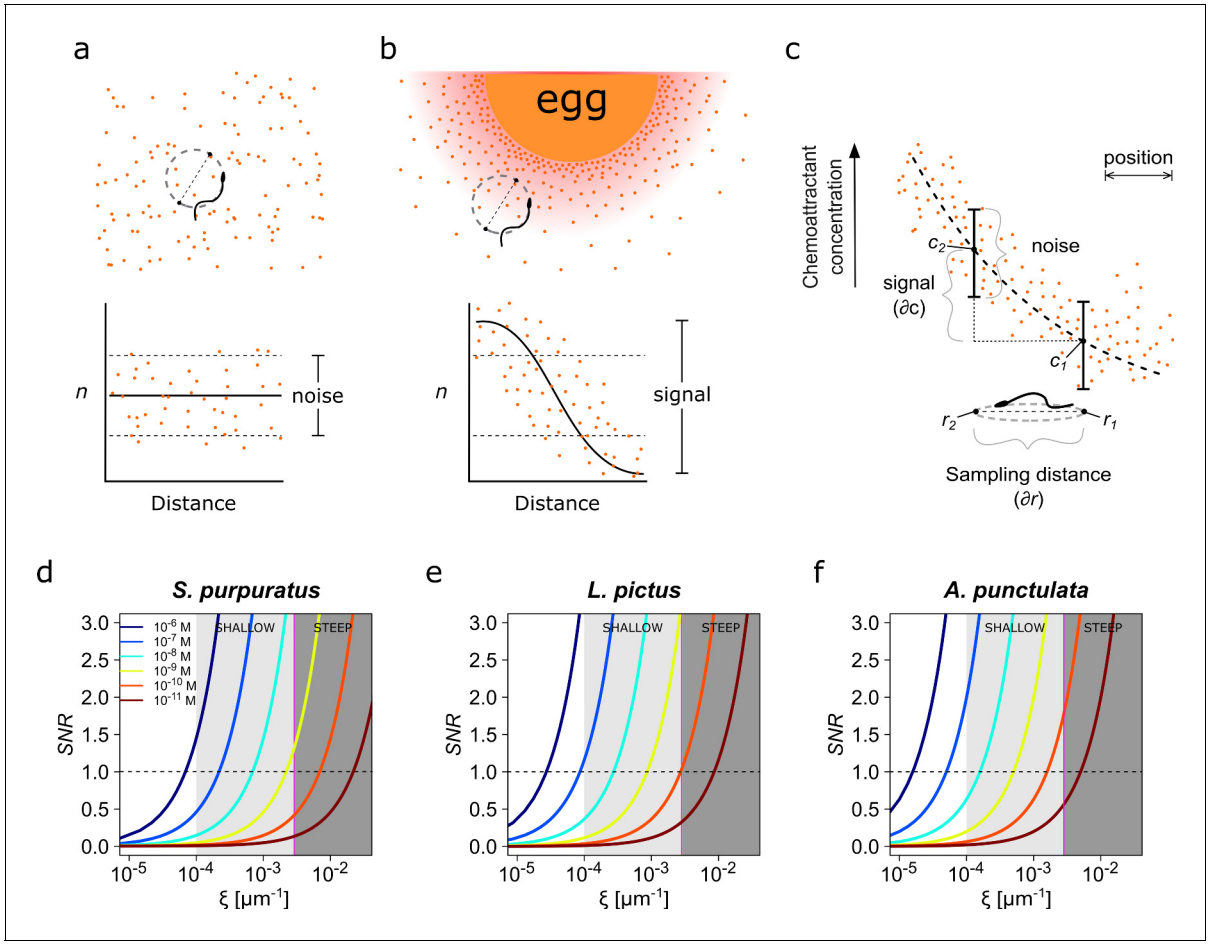

Figure 1. Physics of chemoreception. (**a**) A spermatozoon swimming in an isotropic chemoattractant concentration field, where the number of molecules detected (**n**) is within the noise of detection. (**b**) A spermatozoon swimming near to an egg, while chemoattractant molecules are diffusing from its surrounding jelly layer creating a chemoattractant gradient. Note that the signal detected in this case is larger than the detection noise. (**c**) The assessment of a chemoattractant concentration gradient requires that the signal difference ∂c between two sampled positions ∂r must be greater than the noise. (**d–f**) The signal-to-noise ratio in the determination of the chemoattractant gradient *SNR* plotted against the relative slope of the chemoattractant concentration gradient in log scale, $\xi = \bar{c}^{-1}\frac{\partial c}{\partial r}$, for different chemoattractant concentrations of speract for either *S. purpuratus* (**d**), or *L. pictus* (**e**) spermatozoa, and of resact for *A. punctulata* (**f**) spermatozoa (see ***Supplementary file 1*** for the list of parameter values taken in consideration for panels **d–f**). *S. purpuratus* spermatozoa have lower capacity of detection for the same chemoattractant concentrations at a given ξ than *L. pictus* and *A. punctulata*. The tone of the shaded areas indicates shallow or steep gradient conditions. The horizontal dotted line represents *SNR* = 1; the vertical magenta line represents $\xi = 2.6 \times 10^{-3}$ μm^{-1}. Colors of the line traces (from blue to brown) indicate distinct chemoattractant concentrations in the range [10^{-6} – 10^{-11} M].

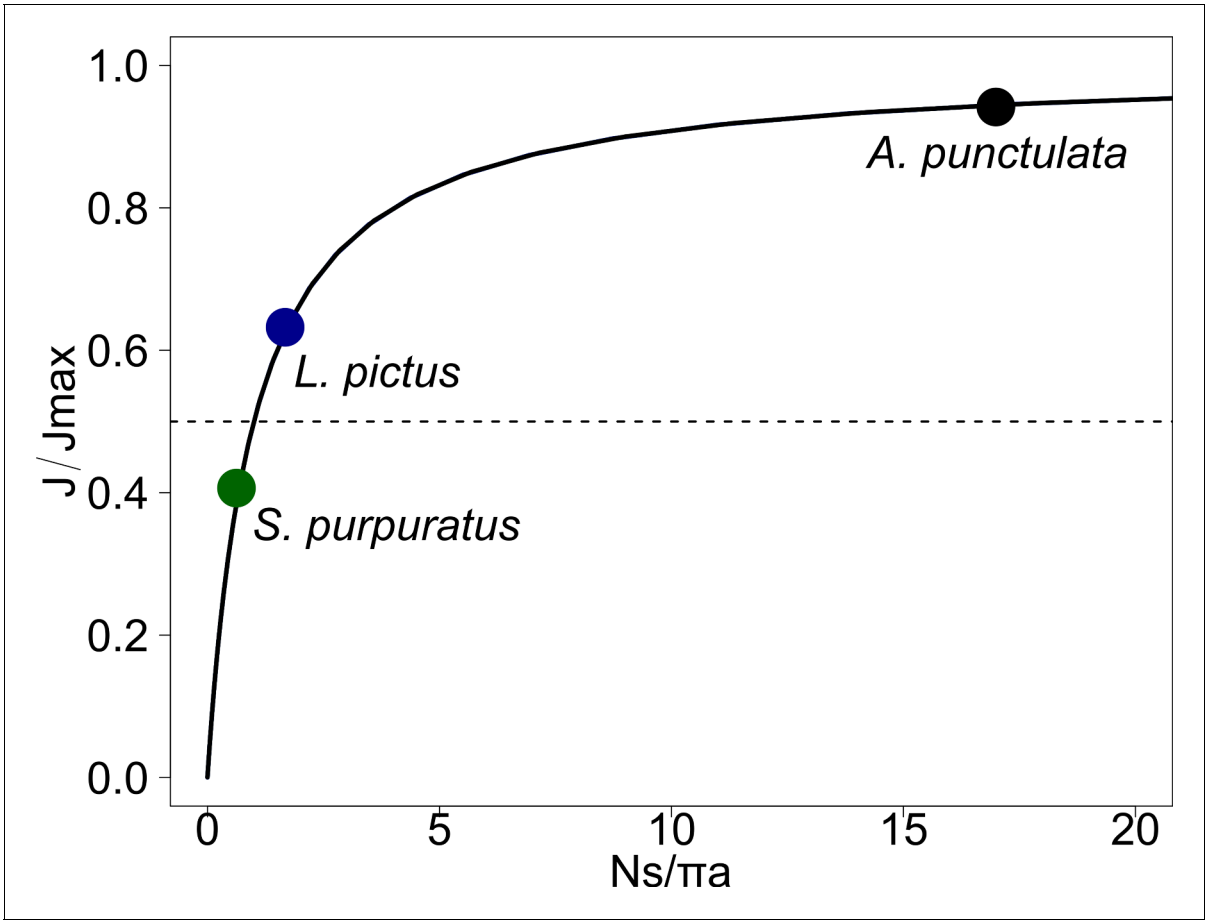

Figure 1—figure supplement 1. Chemoattractant diffusive currents have a non-linear relationship to receptor coverage. For a spherical cell of radius *a*, with *N* disk-like receptors of effective radius *s*, the diffusive current saturates for $N >> N_{1/2} = \pi a/s$ ($N_{1/2}$ is highlighted for *S. purpuratus*, *L. pictus* and *A. punctulata* with a green, blue and black dots, respectively). For *S. purpuratus*, however, the number of receptors is smaller than $N_{1/2}$ and the diffusive influx falls into an almost linear regime.

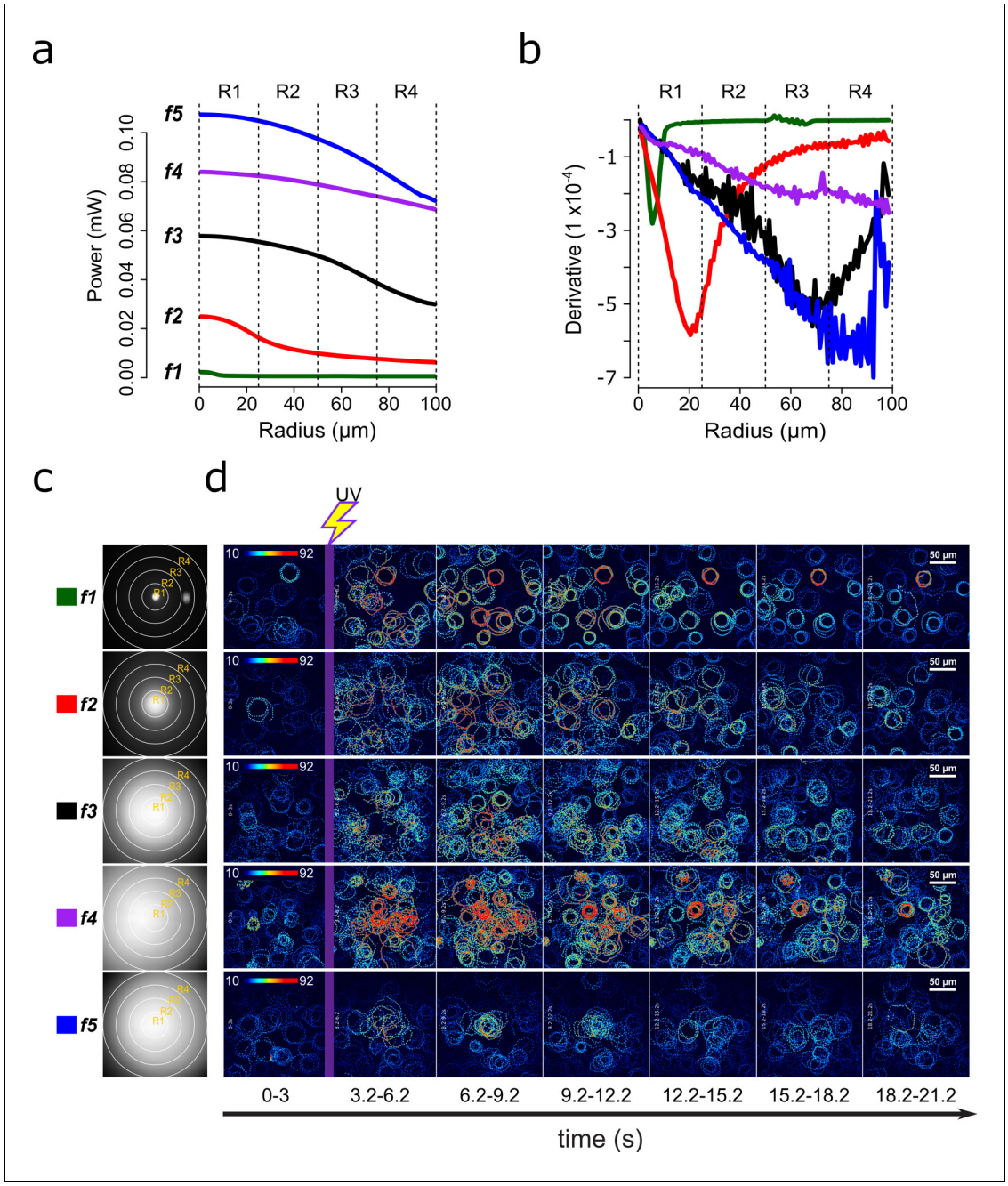

Figure 2. Screening of speract concentration gradients. (**a**) Radial profile and its derivative (**b**) of the UV light scattered at the glass-liquid interface for each optical fiber (f1–f5). (**c**) Spatial distribution of the UV flash energy for each fiber. (**d**) Representative motility and $[Ca^{2+}]_i$ responses of *S. purpuratus* spermatozoa exposed to different concentration gradients of speract. F-F_0 time projections, showing spermatozoa head fluorescence at 3 s intervals before and after photoactivation of 10 nM caged speract in artificial seawater with 200 ms UV flash. The pseudo-color scale represents the relative fluorescence of fluo-4, a $[Ca^{2+}]_i$ indicator, showing maximum (red) and minimum (blue) relative $[Ca^{2+}]_i$. Scale bars of 50 µm.

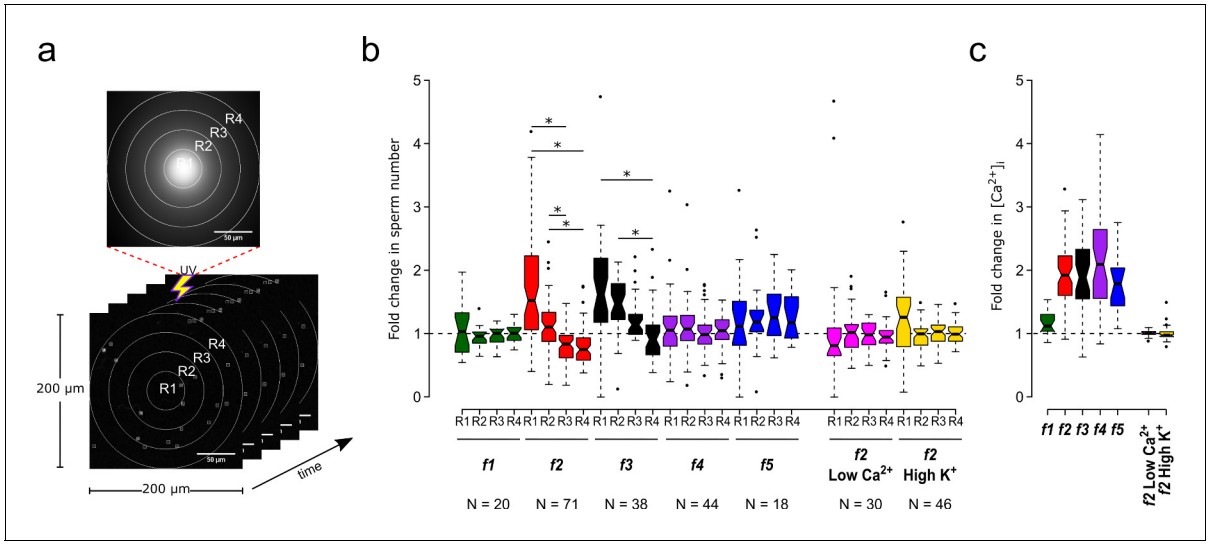

Figure 3. Motility and $[Ca^{2+}]_i$ responses of *S. purpuratus* spermatozoa exposed to specific concentration gradients of speract. (**a**) The positions of the sperm heads within the imaging field are automatically assigned to either R1, R2, R3 or R4 concentric regions around the centroid of the UV flash intensity distribution. Each ROI was also used to obtain the sperm head fluorescence from the raw video microscopy images (as the mean value of the ROI) (see ***Figure 3—figure supplement 1***). Scale bar of 50 µm. (**b**) Fold change in sperm number, defined as the number of spermatozoa at the peak of the response (6 s) relative to the mean number before speract stimulation (0–3 s) (see ***Figure 3—figure supplement 2***). (**c**) Relative changes in $[Ca^{2+}]_i$ experienced by spermatozoa at the peak response (6 s) after speract stimulation. Negative controls for spermatozoa chemotaxis are artificial seawater with nominal Ca^{2+} (Low Ca^{2+}); and artificial seawater with 40 mM of K^+ (High K^+). Both experimental conditions prevent chemotactic responses by inhibiting the Ca^{2+} membrane permeability alterations triggered by speract; the former disrupts the Ca^{2+} electrochemical gradient, and the later disrupt the K^+ electrochemical gradient required as electromotive force needed to elevate pH_i, and to open Ca^{2+} channels. The central line in each box plot represents the median value, the box denotes the data spread from 25% to 75%, and the whiskers reflect 10–90%. The number of experiments is indicated on the bottom of each experimental condition. We used the same number of experiments for the relative change in $[Ca^{2+}]_i$ (right panel). *Statistical significance, $p<0.05$; multiple comparison test after Kruskal-Wallis.

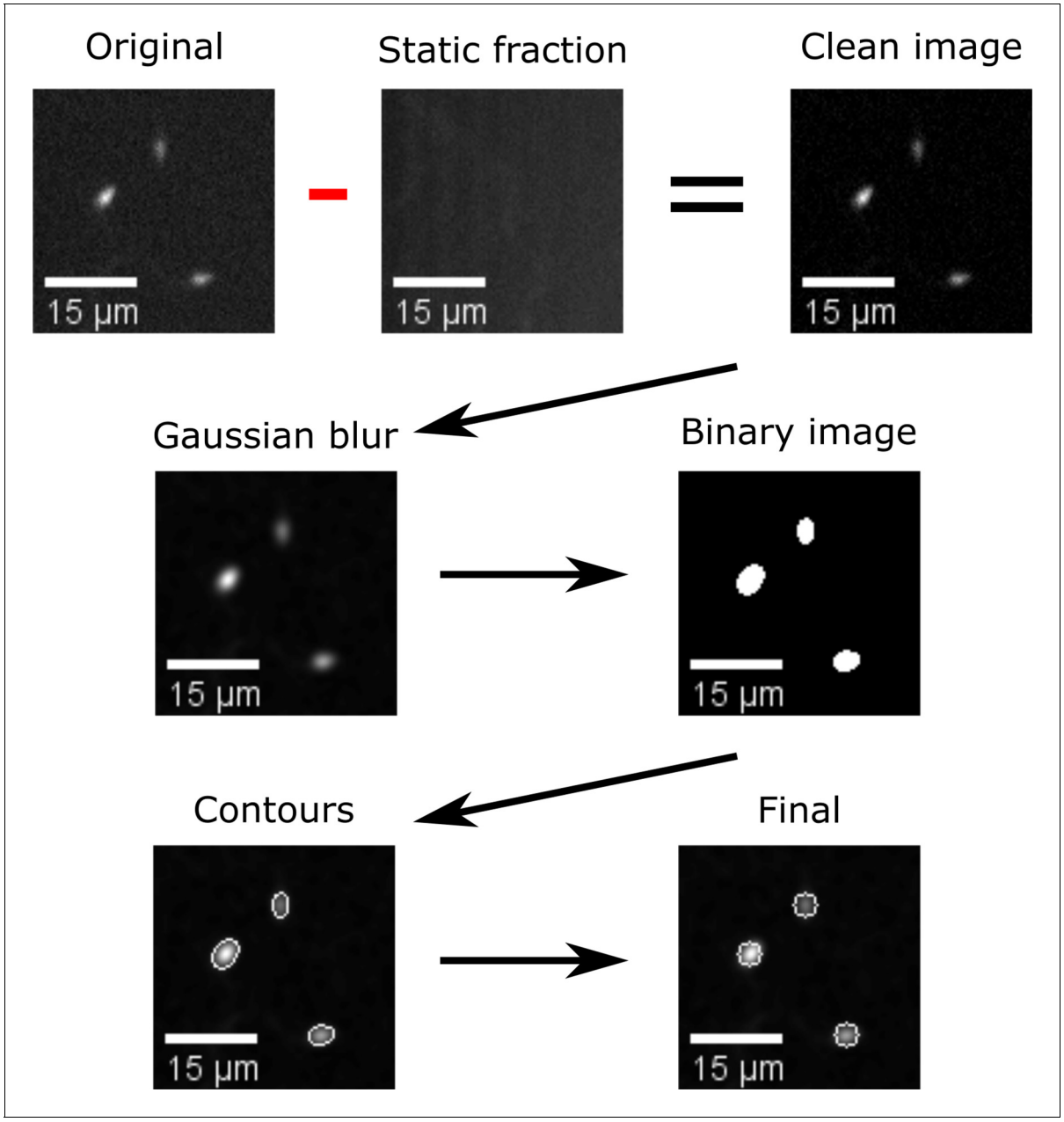

Figure 3—figure supplement 1. Automatic segmentation of swimming spermatozoa. Work-flow of the segmentation algorithm: Video microscopy images were background subtracted by removing the temporal average intensity projection (static fraction) of the un-stimulated frames (93 frames = 3 s), from the whole video (25 s). The resulting images were convolved with a low-pass spatial frequency filter to reduce noise (detector, electronic, shot). The resulting images were thresholded to generate arrays of regions of interest (ROIs), a heuristic search for connected components was then applied to label single ROIs and to assign the corresponding pixels to unique spermatozoa. Scale bar of 15 µm.

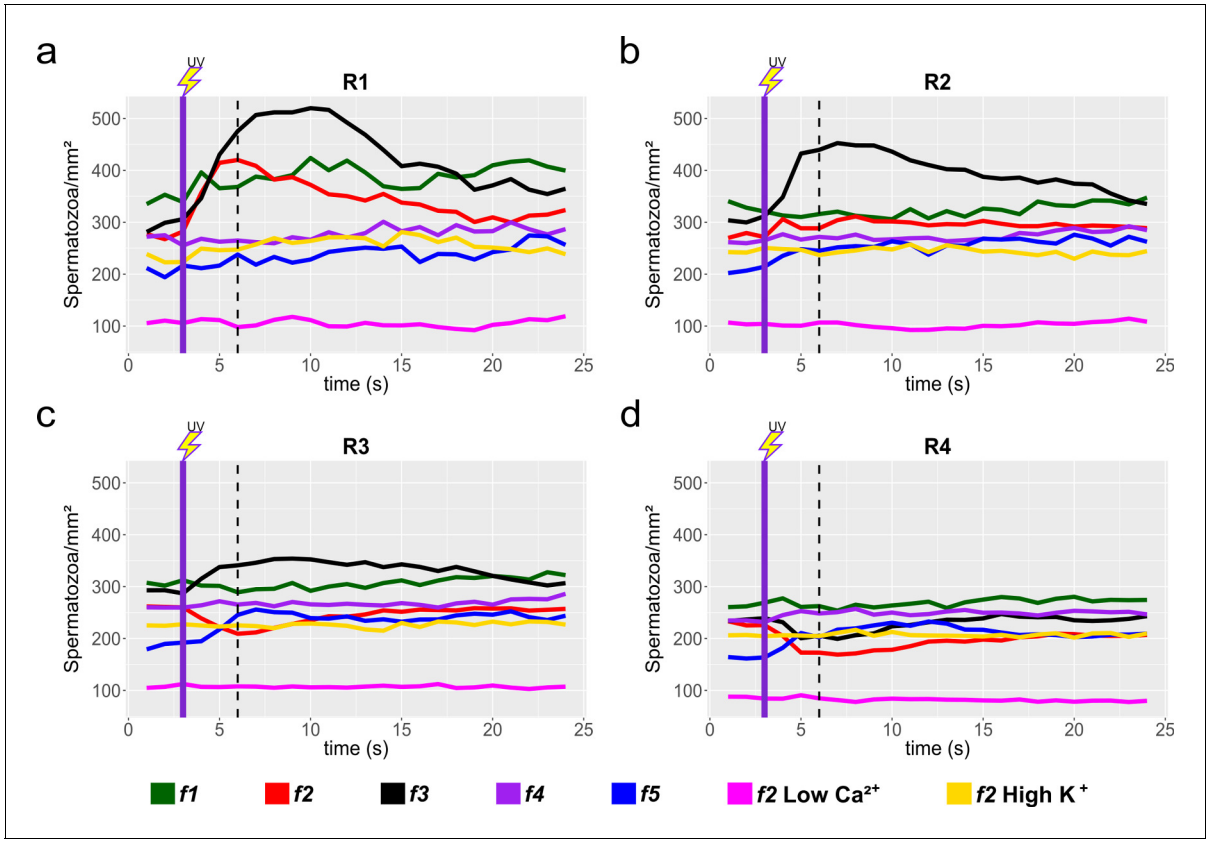

Figure 3—figure supplement 2. Sperm response to speract photo-release, collated data from individual experiments. Sperm motility responses to different speract concentration gradients (f1, f2, f3, f4, f5) at R1 (**a**), R2 (**b**), R3 (**c**) and R4 (**d**) concentric regions (see ***Figure 3a***). Negative controls for sperm chemotaxis are artificial sea water with nominal 0 Ca^{2+} (Low Ca^{2+}); and artificial sea water with 40 mM of K^+ (High K^+). Each time trace represents the mean sperm density from up to 20 video microscopy experiments. Note that peak responses occurred around 6 s (shown by the vertical dashed lines), some 3 s after speract exposure (indicated as vertical dotted lines). Purple vertical line indicates the UV flash (200 ms).

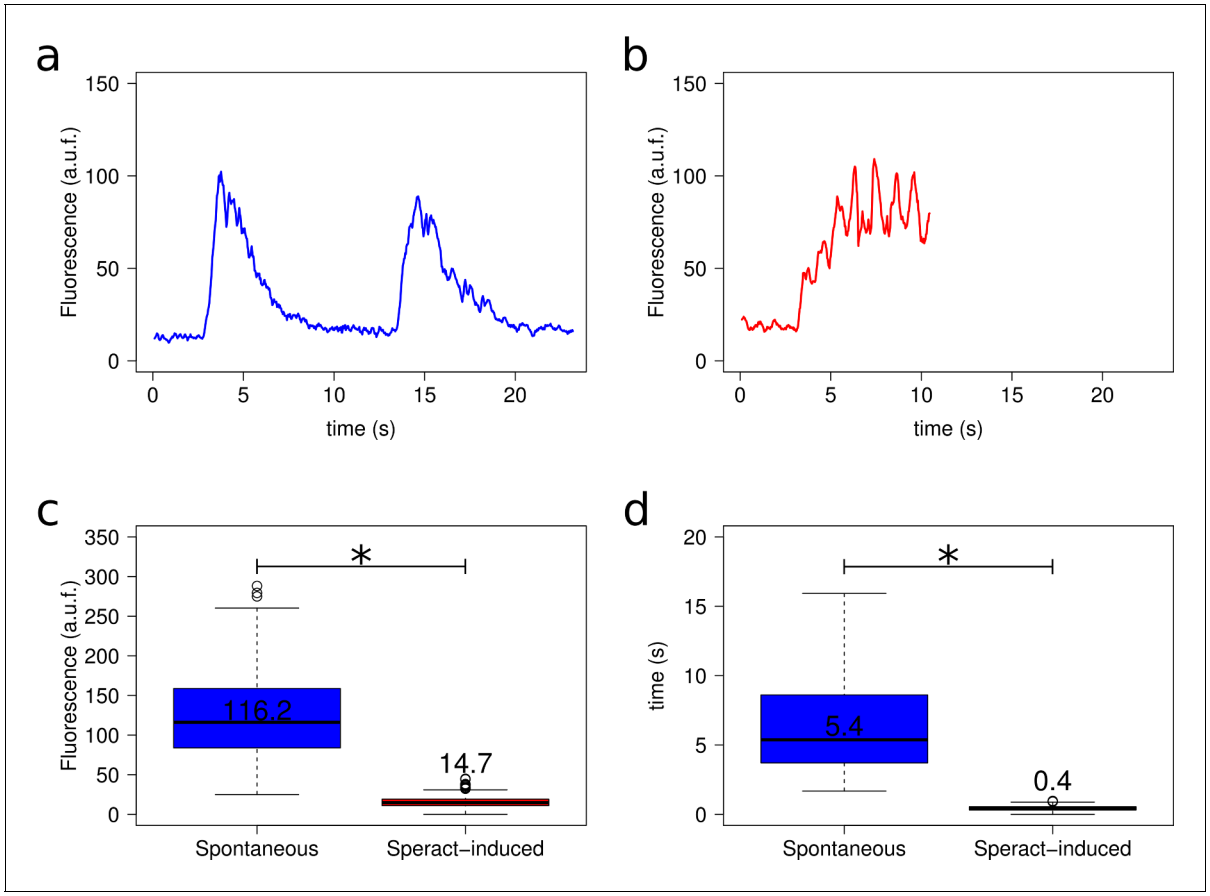

Figure 3—figure supplement 3. Spontaneous *vs.* speract-induced $[Ca^{2+}]_i$ oscillations. (**a**) Example of a spontaneous Ca^{2+} oscillation (two oscillations). Only 20% of sperm experiencing spontaneous oscillations suffer more than one oscillation, most of them experience only one $[Ca^{2+}]_i$ increase. (**b**) Representative trace of speract-induced oscillations. Caged-speract was released after third second. (**c**) Comparison of Ca^{2+} oscillation amplitude between spontaneous (blue) *vs.* speract-induced (red) oscillations. n = 75 for spontaneous and n = 56 for speract-induced oscillations. (**d**) Comparison of Ca^{2+} oscillation period between spontaneous (blue) *vs.* speract-induced (red) oscillations. n = 16 for spontaneous and n = 56 for speract-induced oscillations. *Statistical significance, $p<0.01$, Mann-Whitney *U* test. $[Ca^{2+}]_i$ oscillation traces (panels **a** and **b**) were smoothed using an average filter with a four frame window in a 30.8 fps setting. For further information see Extended Materials and methods, section 2.8. Spontaneous vs. speract-induced $[Ca^{2+}]_i$ oscillations.

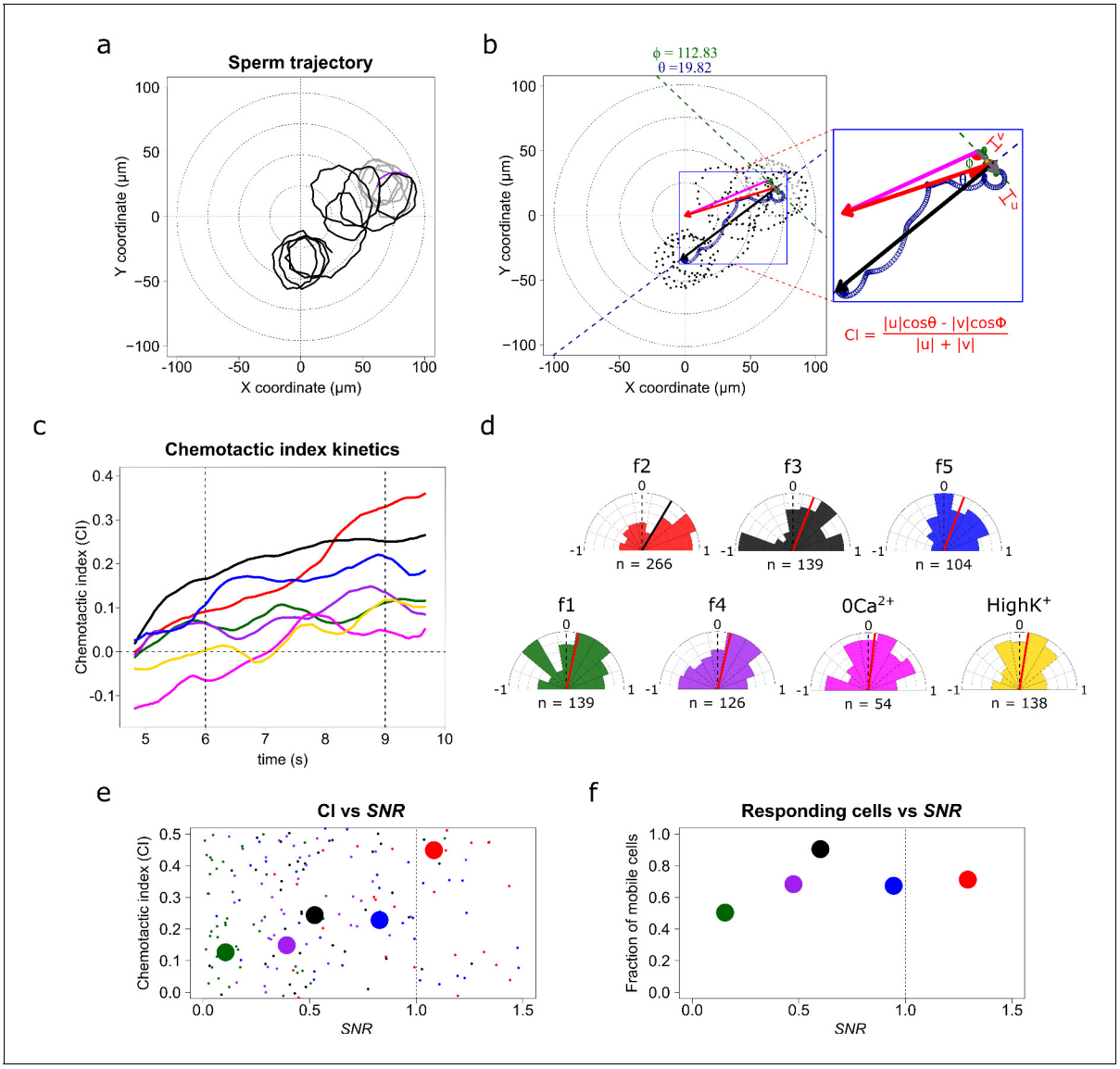

Figure 4. *S. purpuratus* spermatozoa selectively experience chemotaxis toward specific speract gradients. (**a**) Sperm trajectory before (gray) and after (black) the UV irradiation (purple). (**b**) Definition of a chemotactic index to score chemotactic responses. Dots represent sperm trajectory before (gray) and after (black) UV irradiation. Green and blue empty spirals indicate the smoothed trajectory before and after UV irradiation. Gray and black vectors are the progressive sperm displacement before and after stimulation, respectively; and the v and u vectors are the linear speed before and after stimulation; and ϕ and θ are the angles to their corresponding reference vectors to the center of the imaging field – the highest UV irradiated area, (magenta and red, respectively). Chemotactic index (CI) is defined as in the inset (see also ***Video 2***). (**c**) Temporal evolution of the chemotactic index. Functions were calculated from the median obtained from sperm trajectories of each of *f1, f2, f3, f4, f5, f2-ZeroCa*$^{2+}$, and *f2-HighK*$^{+}$ experimental conditions (***Appendix 1—video 7***). (**d**) Radial histograms of CI computed at second 9 (vertical dotted line at panel **c**). Significant differences (*Binomial test, p-value<0.05*) were observed only for *f2, f3* and *f5* fibers, compared to controls. n represents the number of individual sperm trajectories analyzed. (**e**) CI as a function of the signal-to-noise ratio (*SNR*). Each parameter was calculated for single cells. Large filled points represent the median for each gradient condition distribution. (**f**) Fraction of responding cells as a function of the *SNR* (spermatozoa whose effective displacement was above the unstimulated cells). The apparent diffusion of the swimming drifting circle of unstimulated *S. purpuratus* spermatozoa is $D_{app} = 9 \pm 3\ \mu m^2\ s^{-1}$ (***Friedrich, 2008***; ***Friedrich and Jülicher, 2008***; ***Riedel et al., 2005***), here responsive cells were considered by showing a $D_{app} = 9\ \mu m^2\ s^{-1}$, and were evaluated at second 9.

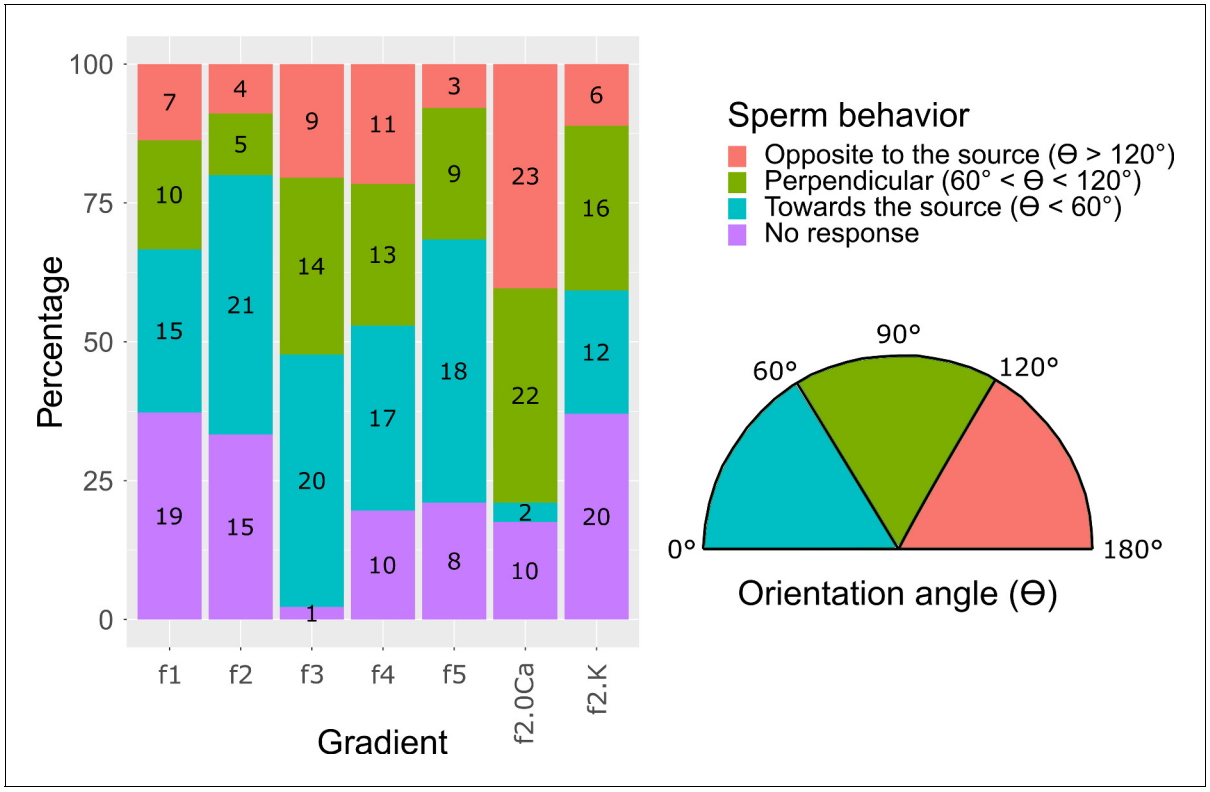

Figure 4—figure supplement 1. Sperm swimming behavior in response to different chemoattractant gradients. *S. purpuratus* sperm behavior classified in four different classes: i) No response (purple), when spermatozoa keep swimming in concentric circles and do not move more than 15 μm of progressive swimming; ii) Toward the chemoattractant source (cyan), when spermatozoa respond drifting in swimming circles with an orientation angle (θ) smaller than 60˚ ($\theta < 60$˚); iii) Opposite to the chemoattractant source (pink), when spermatozoa respond drifting in swimming circles with an orientation angle (θ) bigger than 120˚ ($\theta > 120$˚); and iv) Perpendicular to the chemoattractant source (green), when spermatozoa respond drifting in swimming circles with an orientation angle (θ) smaller than 120˚ but bigger than 60˚ (60˚ $\leq \theta \leq 120$˚). The orientation angle θ is defined as the swimming angle of the drifting circles after speract uncaging (see ***Figure 4b***). This analysis was made at second six after speract uncaging. Numbers in each bar represent the number of spermatozoa in each condition. Inset at the right panel shows the orientation angles (θ). For further information see Extended Materials and methods, section 2.7. Sperm swimming behavior in different chemoattractant gradients.

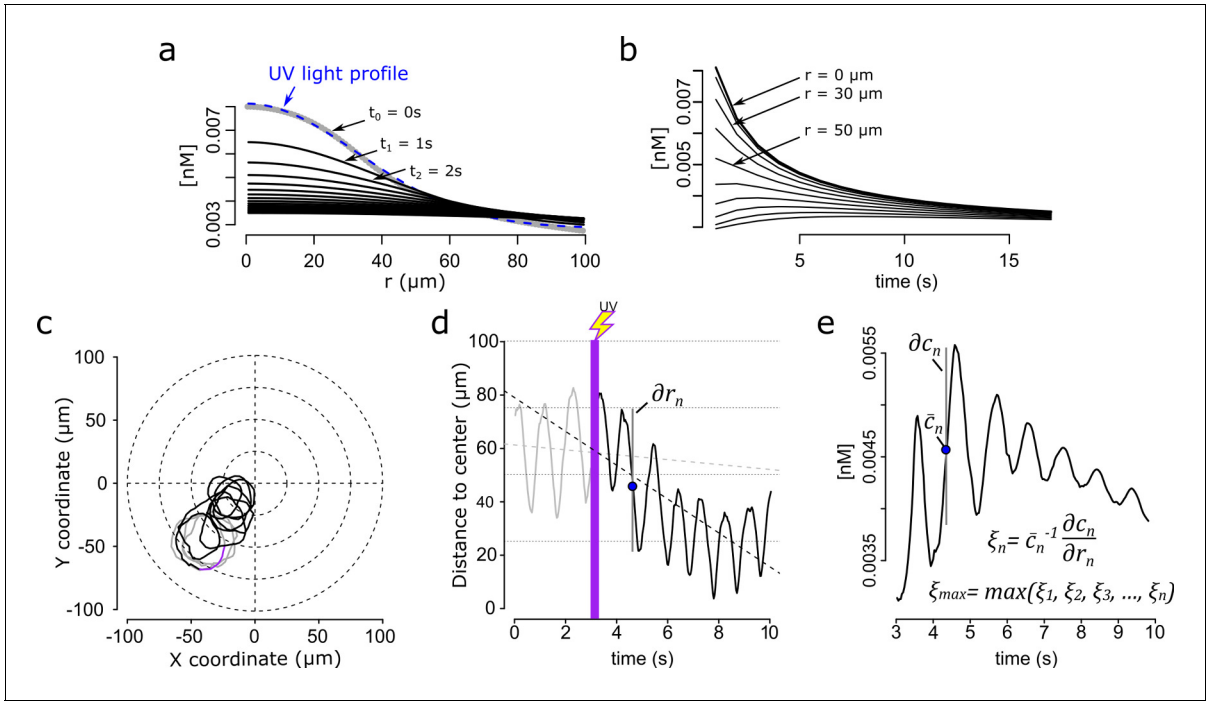

Figure 5. Steep speract gradients provoke chemotaxis in *S. purpuratus* spermatozoa. a. Dynamics of the *f2* speract gradient. The blue dashed line (t_0 = 0 s) corresponds to a Gaussian distribution fitted to the UV light profile and illustrates the putative shape of the instantaneously-generated speract concentration gradient. Solid black lines illustrate the temporal evolution of the speract concentration field after t = 1, 2, 3, …, 20 s. (**b**) Temporal changes in the *f2* speract field computed radially (each 10 μm) from the center of the gradient. (**c**) Characteristic motility changes of a *S. purpuratus* spermatozoon exposed to the *f2* speract gradient. Solid lines illustrate its swimming trajectory 3 s before (gray), during UV flash (purple) and 6 s after (black) speract exposure. (**d**) Spermatozoa head distance to the source of the speract gradient versus time, calculated from sperm trajectory in (**c**). (**e**). Stimulus function computed from the swimming behavior of the spermatozoon in (**c**), considering the dynamics of (**a** and **b**).

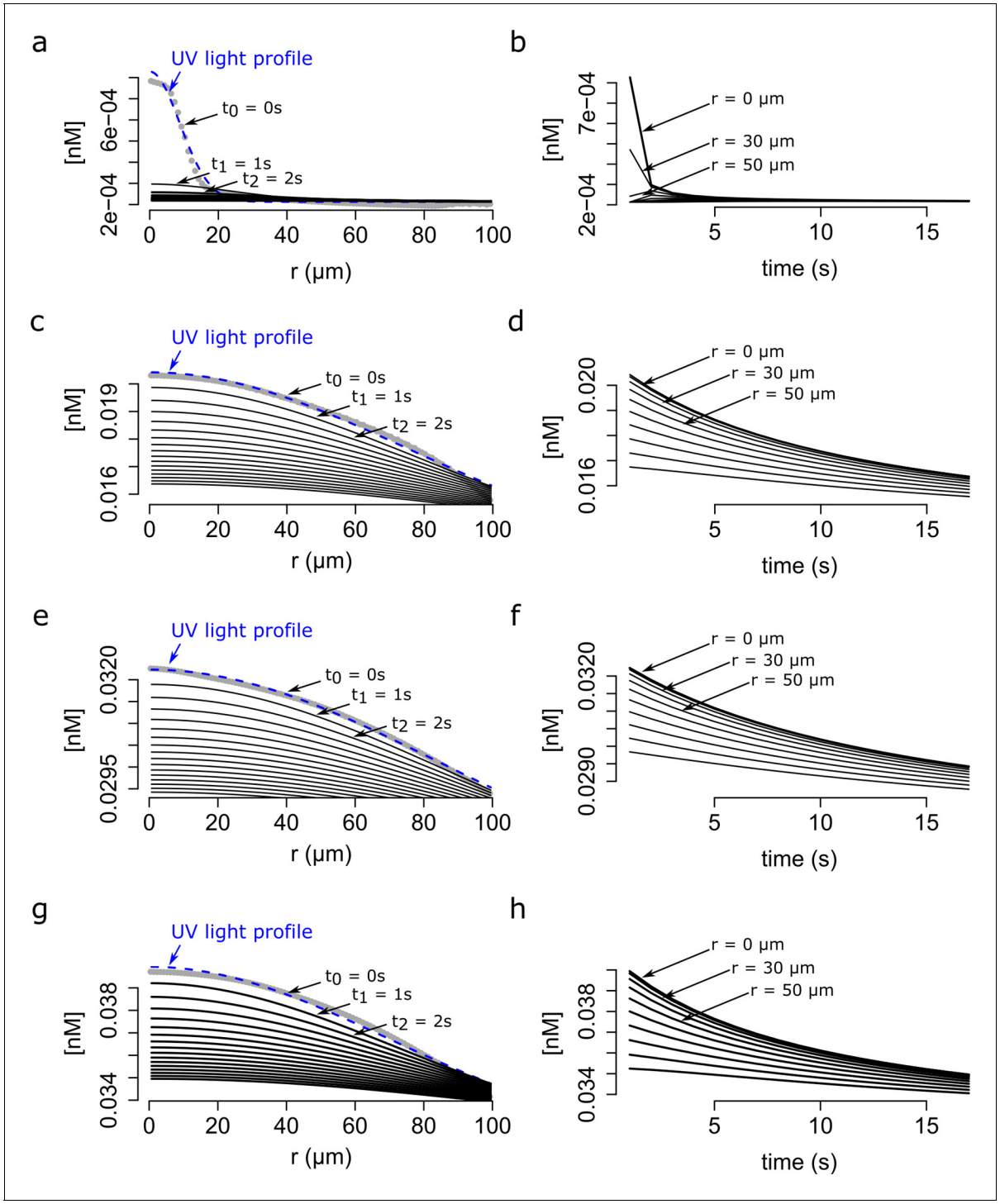

Figure 5—figure supplement 1. Modeling of the dynamics of speract gradient based on the UV light profile of distinct optical fibers. The radial profiles of the UV light scattered at the glass-liquid interface of *f1*, *f3*, *f4*, *f5* optical fibers are shown in gray. The speract gradient was generated as in ***Figure 5***, but with the corresponding *f1* (**a and b**), *f3* (**c and d**), *f4* (**e and f**) and *f5* (**g and h**) optical fibers. *Left panels* - The dynamics of the speract gradient computed as is in ***Figure 5***. The blue dashed line ($t_0 = 0$) corresponds to a Gaussian distribution fitted to the UV light profile, and illustrates the putative shape of the instantaneously generated speract gradient. Solid black lines illustrate the shape of the speract gradient after t = 1, 2, 3, . . ., 20 s. *Right panels* - Simulated temporal changes in speract concentration gradients of *f1* (**a**), *f3* (**c**), *f4* (**e**) and *f5* (**g**) at each 10 μm radial point from the center of the concentration gradient.

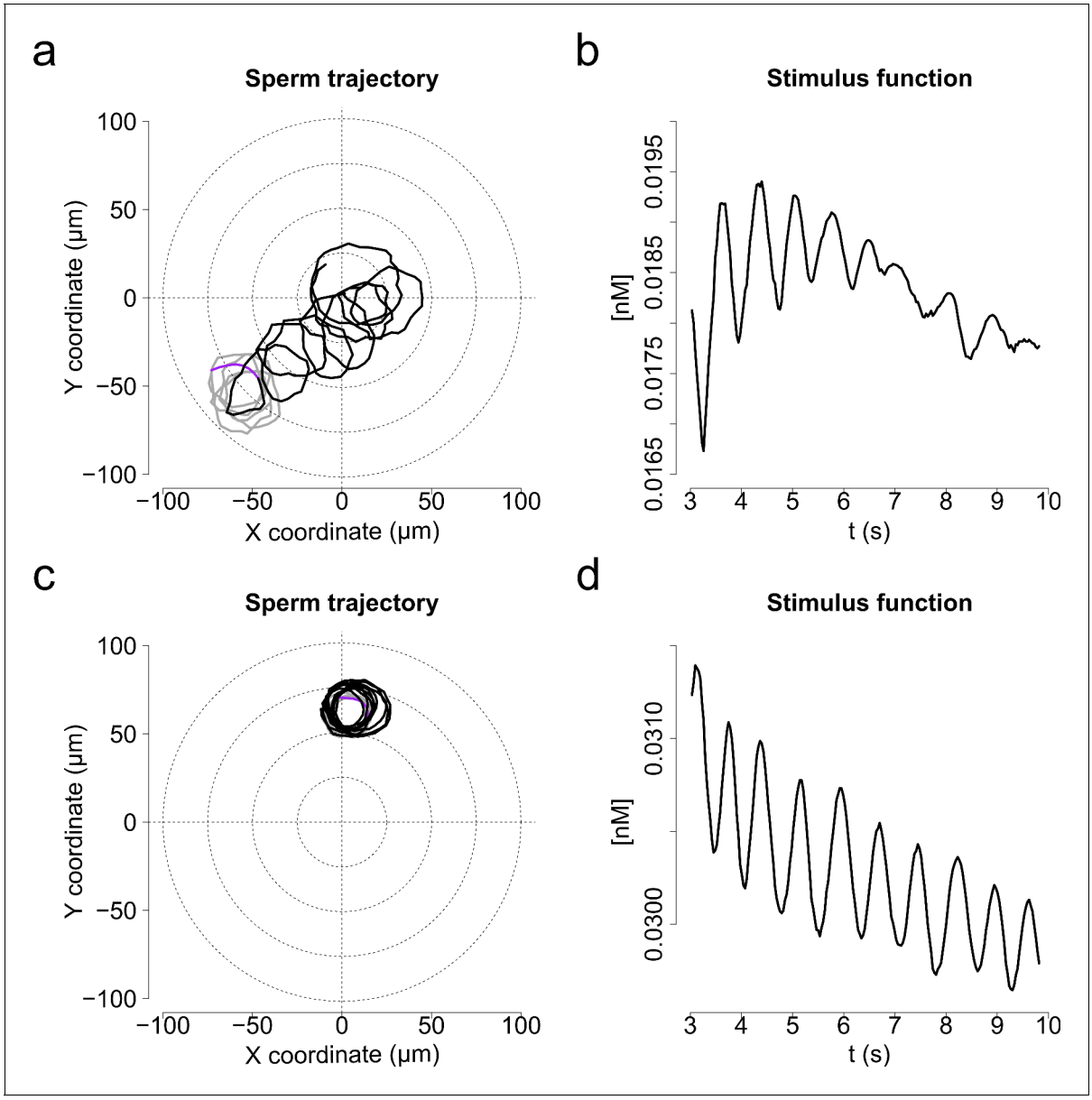

Figure 5—figure supplement 2. Characteristic motility changes of a *S. purpuratus* spermatozoon exposed to *f3 and f4* speract gradients (chemotactic *vs.* non-chemotactic response). Panels (**a** and **b**) show single cell responses to the *f3* speract gradient (chemotactic); and panels **c**) and **d**) to the *f4* speract gradient (non-chemotactic). (**a, c**) Solid lines illustrate the spermatozoon swimming trajectory 3 s before (gray) and 6 s after (black) speract gradient exposure. (**b, d**). Stimulus function computed from (**a** and **c**), considering the spatio-temporal dynamics of speract computed for the *f3* and *f4* gradients, respectively.

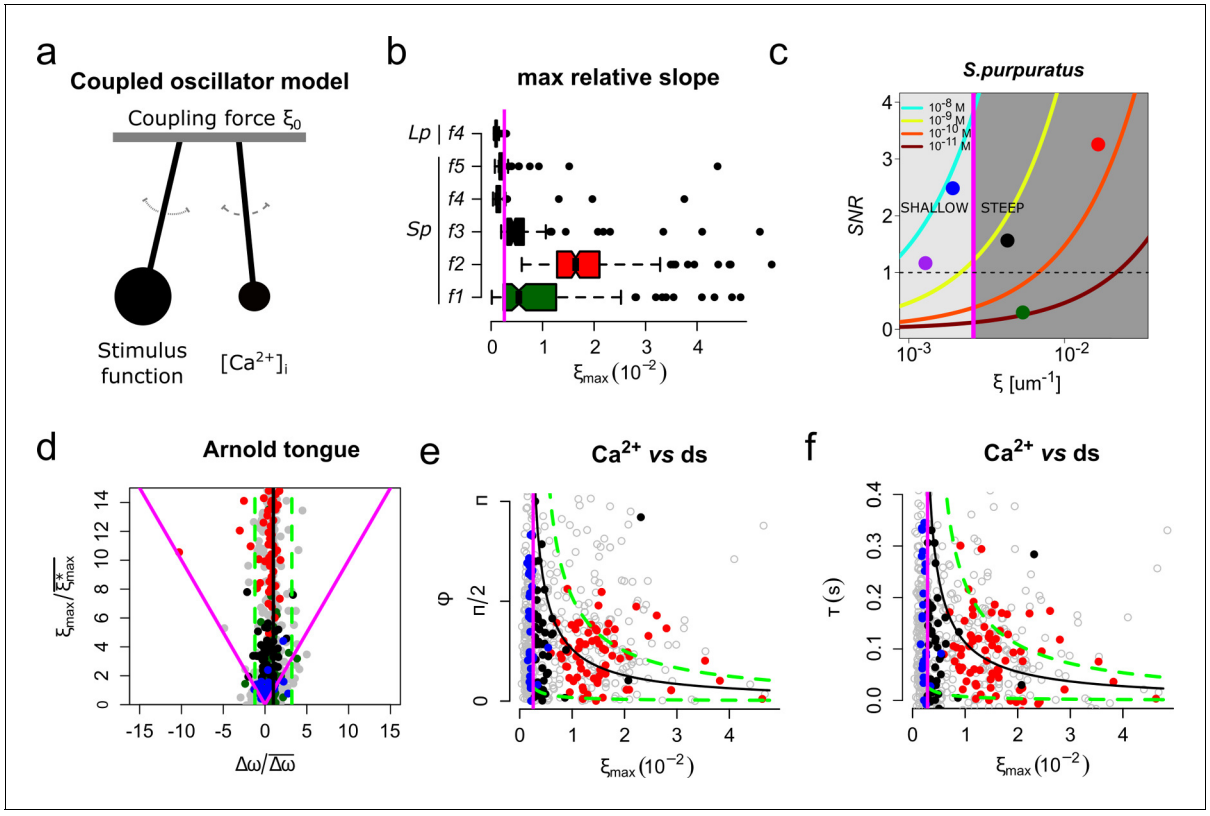

Figure 6. The slope of the speract concentration gradient generates a frequency-locking phenomenon between the stimulus function and the internal Ca^{2+} oscillator triggered by speract. (**a**) Coupled oscillator model. Each sperm has two independent oscillators: i) stimulus function and ii) $[Ca^{2+}]_i$, which can be coupled through a forcing term that connects them, in our case the slope of the chemoattractant concentration gradient (ξ_0). (**b**) Maximum relative slopes (ξ_{max}) of the chemoattractant concentration gradient experienced by *S. purpuratus* (*Sp*) spermatozoa when exposed to *f1*, *f2*, *f3*, *f4*, *f5* speract gradients. The maximum relative slopes of the chemoattractant concentration gradient experienced by *L. pictus* spermatozoa (*Lp*) toward *f4* experimental regime are also shown. Note that ξ_{max} for *f2*, *f3*, and *f5*, are up to 2–3 times greater than in *f4*, regardless of the species. (**c**) Experimental signal-to-noise ratios (*SNR*) regimes experienced by spermatozoa swimming in different gradient conditions. Note that only *f2*, *f3* and *f5* have higher *SNR*, compared to other gradient conditions, for which stochastic fluctuations mask the signal. This *SNR* calculation assumes a 10% of speract uncaging. The maximum relative slopes (ξ) are shown in log scale (**d**) Arnold's tongue indicating the difference in intrinsic frequency of the internal Ca^{2+} oscillator of *S. purpuratus* spermatozoa, just before and after the speract gradient exposure. (**e**). Phase difference between the time derivative of the stimulus function and the internal Ca^{2+} oscillator of *S. purpuratus* spermatozoa, obtained by computing the cross-correlation function between both time series (***Figure 6—figure supplement 2***). (**f**). Phase difference between the time derivative of the stimulus function and the internal Ca^{2+} oscillator of *S. purpuratus* spermatozoa expressed in temporal delays. (**d-f**) Gray points represent the collated data of all *f1*, *f2*, *f3*, *f4*, *f5* experimental regimes. Red, black and blue points indicate chemotactic spermatozoa (CI > 0 at second three after UV flash), located in R3, and R4 regions just before the speract gradient is established under *f2*, *f3* and *f5* experimental regimes, respectively. Magenta lines represent the transition boundary ($\gamma_{min} = \overline{\xi^*_{max}} \sim 2.6\times10^{-3}$ μm^{-1}, see also ***Figure 1d–f***) below which no synchrony is observed, obtained from the theoretical estimates (black curves, mean of $\Delta\omega$) of panels (**e**) and (**f**). Green dashed lines indicate confidence intervals (mean ± standard deviation).

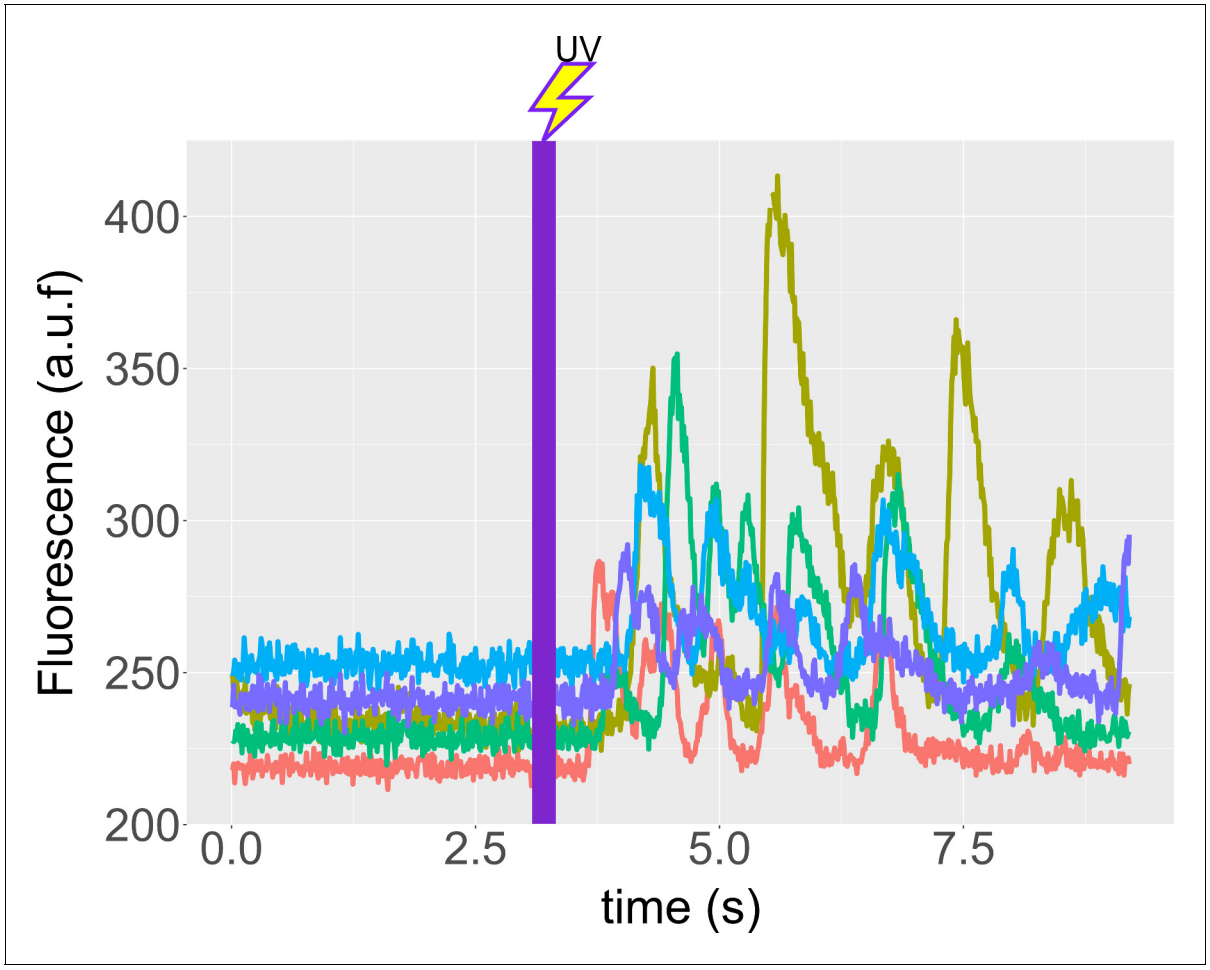

Figure 6—figure supplement 1. Speract induces Ca^{2+} oscillations in immobilized *S. purpuratus* spermatozoa. Spermatozoa were immobilized on cover slips coated with poly-D-lysine (see Materials and methods), and ASW containing 500 nM caged speract added. Recordings were performed 3 s before and during 6 s after 200 ms of UV irradiation. *f4* optical fiber was used for the UV light path, to generate the speract concentration gradient. Time traces indicate the $[Ca^{2+}]_i$ of selected spermatozoa of ***Appendix 1—video 8***. Note that the photo-release of speract induces a train of $[Ca^{2+}]_i$ increases in immobilized spermatozoa, and hence provides evidence for the presence of an internal Ca^{2+} oscillator triggered by speract.

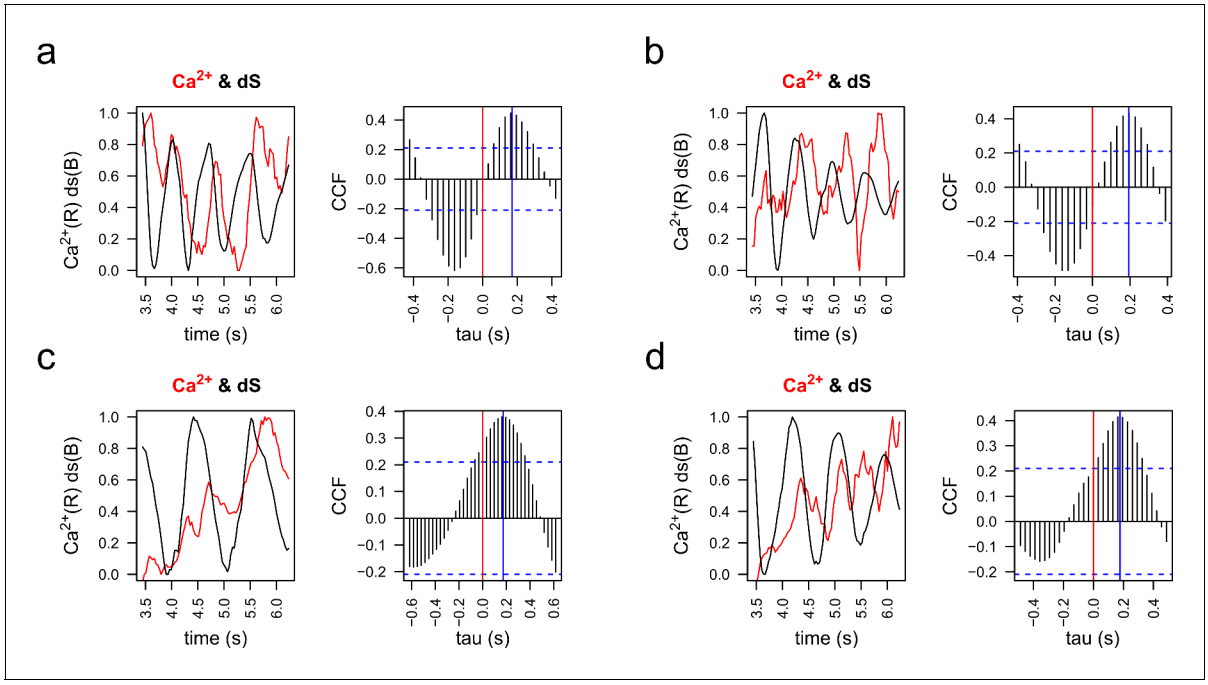

Figure 6—figure supplement 2. Cross-correlation analysis of $[Ca^{2+}]_i$ and stimulus function derivative (dS) signals. Representative examples of $[Ca^{2+}]_i$ (red) and the derivative of the stimulus function (dS) (black) were plotted and then analyzed by cross-correlation analysis (CCF). Red vertical lines indicate the zero, blue vertical lines indicate the point of maximum correlation for each case, which means that the phase shifting between $[Ca^{2+}]_i$ and dS is around 200 ms in these cases. Examples of a pair of spermatozoa for the two principal chemotactic gradients (f2 and f3) are shown. (**a, b**) Representative examples of two spermatozoa in an *f2* gradient. (**c, d**) Representative examples of two spermatozoa in an *f3* gradient.